Ultrasonics 94 (2019) 82–91

Contents lists available at ScienceDirect

Ultrasonics

journal homepage: www.elsevier.com/locate/ultras

Experimental characterization of synthetic porous orthorhombic fractured medium: A physical modeling approach

Crislene Silva[a], J.J.S. de Figueiredo[a,b,*], Tatiana Chichinina[c], Murillo J.S. Nascimento[a], Leo Kirchhof[a]

[a] Faculty of Geophysics, Federal University of Pará, Petrophysics and Rock Physics Laboratory – Prof. Dr. Om Prakash Verma, Belém, PA, Brazil
[b] National Institute for Petroleum Geophysics (INCT-GP), Brazil
[c] Instituto Mexicano del Petroleo, Ciudad de México, MX, Mexico

ARTICLE INFO

Keywords:
Orthorhombic medium
Fractures
Physical modeling
Ultrasonic waves

ABSTRACT

The study of fractures in subsurface is very important since they are, in some cases, the main conduits for hydrocarbon flow in a reservoir. There are many ways to study the behavior of seismic waves in different fracturing conditions, including the use of physical modeling. This method allows, among other approaches, the analysis of the behavior of seismic wave properties in complex fractured media, such as media with orthorhombic symmetry. In this work we performed ultrasonic measurements on fractured physical models with orthorhombic symmetry from which we analyzed the behavior of elastic velocities and anisotropy parameters for different number of fractures. The presented results show the efficiency of the construction methodology used in the study by presenting P- and S- wave velocity values consistent with the theory for an orthorhombic medium. It was observed that for the direction perpendicular to the fracture system the values of P and S-wave velocities were the smallest for each model, and that the velocities decreased as the number of fractures increased in all models. Furthermore, most of the ϵ and γ values show a decreasing behavior as a function of the decreasing number of cracks, being the trend curves of ϵ linear and most of the trend curves of γ quadratic. Additionally, all the ϵ parameters presented a high correlation with the γ parameters for a small number of fractures, lower than 5.

1. Introduction

In the hydrocarbon exploration process it is highly important to characterize the reservoir in study. This characterization involves the determination of physical and petrophysical characteristics of the reservoir, such as porosity and permeability, as well as the study of the fractures existing in it. Fractures are defined as any discontinuity existing in subsurface. They can have several different sizes, apertures and orientations and they are a key factor in hydrocarbon production, mainly in unconventional reservoirs, since they are hydrocarbon conduits. Thus, it is of vital importance to study their properties, such as fracture orientation, density and aspect ratio, in order to optimize fluid production in a reservoir [26,33]. The main issue rises when the study of fractures and cracks are related to the anisotropy induced by them. Depending on the type of anisotropy the study of these media may be a hard task.

Studies about the influence of fractured media in seismic wave propagation have been widely reported throughout the years. Early studies used both seismological and synthetic data to describe the behavior of seismic waves in fractured media, including the shear-wave splitting phenomenon [9,10,36]. These studies showed the possibility of using seismic waves as tools for fracture characterization. There are many ways to analyze the influence of rock properties, including fracture characteristics, in the behavior of seismic waves. One way is using numerical modeling, which is the simulation of seismic wave propagation through a medium with controlled physical properties. This process is performed using numerical methods, such as finite elements or finite differences. From the numerical modeling results it is possible to analyze how traveltime and amplitude, among other properties, vary for different geological conditions. Another way of analyzing the behavior of seismic waves for different fracture properties is using effective medium theories [21,22], which are equations that describe the macroscopic characteristics of a composite material from properties which are averages of the multiple values of the constituents that directly make up the material, for example, how P- and S-wave velocities and/or anisotropy parameters vary in terms of fracture shape, fracture

* Corresponding author.
E-mail address: jadsomjose@gmail.com (J.J.S. de Figueiredo).

https://doi.org/10.1016/j.ultras.2018.11.015
Received 23 May 2018; Received in revised form 28 November 2018; Accepted 30 November 2018
Available online 06 December 2018
0041-624X/

density or fracture filling materials. In addition to these two ways of describing the influence of fractures in seismic waves, the physical modeling process can also be used with this purpose. Physical modeling is the attempt to simulate real rocks through the construction of synthetic models of small scale and controlled properties [29,30,34,35].

Transmission or reflection experiments [14,15] can be performed on these models using ultrasonic transducers, which are seismic sources with very high frequencies, using the signal obtained from experiments on synthetic models it is possible to carry out a great variety of analyses about the seismic waves for different kinds of rocks (simulating different geological conditions). Both the construction of physical models and the performing of ultrasonic experiments are usually realized in laboratory, with controlled conditions. Among other approaches, studies use physical modeling to analyze how seismic wave properties vary for different saturating fluids [1,13,37] and for different fracturing properties, such as fracture aspect ratio [20], aperture [40], orientation [11,32] and density [12]. The physical models are constructed using different methodologies. Assad et al. [2,4] used epoxy resin and small rubber discs to simulate a vertical transversely isotropic (VTI) sandstone with oriented cracks and analyzed the influence of crack density and aspect ratio in the behavior of both P- and S-waves. Figueiredo et al. [11] used similar materials to construct VTI rocks with different crack densities and crack orientations. Physical models composed by synthetic materials, such as rubber and resin, provide reliable qualitative and quantitative analyses but have some limitations since they preclude the saturation of the models. Moreover, they have properties very distant from the properties of real rocks. To overcome this problem, some authors used more realistic materials to construct the models. Santos et al. [31] used a mixture of sand and cement to create synthetic VTI sandstones. They simulated cracks by empty spaces generated after the dissolution of styrofoam by solvent. Another methodology that produces physical models closer to real rocks is the one proposed by Tillotson et al. [38] where they use a mixture of sand, kaolinite and sodium silicate to create sandstones.

Along with isotropic and VTI media, the physical modeling can be used to reproduce more complex types of structures, such as media with orthorhombic symmetry. Related to these structures, early physical modeling experiments have been performed in order to investigate the influence of fractures in the seismic signal. The majority of these works uses a phenolic material, composed by laminated sheets of canvas fabric bonded together with resin, to simulate the orthorhombic symmetry. Brown et al. [6,8] developed the first orthotropic physical study on a phenolic material by presenting elastic velocities, stiffness coefficients, and anisotropic parameters obtained from ultrasonic measurements in different group angles (0–180°). Chang and Gardner [7] constructed a physical orthorhombic model of three layers in order to analyze the effect of fractures on moveout velocities and wave amplitudes. The intermediate layer of this model is a circular-shaped phenolic cut used to simulate vertical fractures. Assad [3] constructed orthorhombic physical models with two orthogonally superimposed sets of fractures. The first set of fractures was made of rubber inclusions, to simulate fractures filled with weak material, and the second one was made of thin plates of epoxy resin closely spaced. Also, the author constructed an isotropic and a VTI sample to control the reliability of the models. As a result, the article presents the elastic velocities of all three directions of propagation obtained through a pulse transmission method and the calculated the Thomsen's parameters for each sample. Mahmoudian et al. [24]'s physical models were made of cuts of a board of phenolic material, used to simulate sets of fractures, bounded together with epoxy resin, to simulate a VTI background. These samples were characterized using ultrasonic transmission seismograms to pick arrival traveltimes and calculate the group velocities of the qP- and qS-waves. These velocities, in turn, were used to estimate density-normalized stiffness coefficients.

The main objective of this work is to demonstrate, through the analysis of seismic wave velocities and Tsvankin's parameters, the orthorhombicity of the samples constructed. The results by themselves are a demonstration of the effectiveness of the sample construction methodology. One of the advantages of this methodology is that the samples constructed are porous, which makes them more similar to real rocks. The physical models are constructed with a different number of fractures each and their P- and S-wave velocities are estimated from an ultrasonic transmission procedure using 500 kHz S-wave transducers. We present the eventual analysis of how P- and S-wave velocities and their related anisotropy parameter vary in terms of the number of fractures, along with a correlation between all the anisotropy parameters and show a relation among them.

2. Theoretical background

The stiffness matrix $C_{\alpha\beta}$ associated to an orthorhombic medium has nine independent components and is mathematically described by

$$C_{\alpha\beta} = \begin{pmatrix} C_{11} & C_{12} & C_{13} & 0 & 0 & 0 \\ C_{12} & C_{22} & C_{23} & 0 & 0 & 0 \\ C_{13} & C_{23} & C_{33} & 0 & 0 & 0 \\ 0 & 0 & 0 & C_{44} & 0 & 0 \\ 0 & 0 & 0 & 0 & C_{55} & 0 \\ 0 & 0 & 0 & 0 & 0 & C_{66} \end{pmatrix}. \quad (1)$$

This medium has a lower degree of symmetry in comparison with a vertically transversely isotropic (VTI) medium whose stiffness matrix is composed by five independent coefficients. While the VTI medium has one axis of symmetry (in the Z-direction) and one isotropic plane perpendicular to it (the XY-plane), the orthorhombic medium has three mutually perpendicular planes of symmetry. For a VTI medium, there are three wave modes: the longitudinal one called Vp and two transversal waves, the fast, here called Vs_1, and the slow, here called Vs_2 [36]. While for the orthorhombic media, there are tree propagation modes – Vp, Vs_1 e Vs_2 – for each symmetry plane [39]. In addition to that, for a medium to be classified as orthorhombic, Vs_{xy} must be equal to Vs_{yx} and the same must hold for Vs_{zy} and Vs_{yz} and for Vs_{zx} and Vs_{xz}, where the s indicates that these velocities are related to the S-wave, the first subscript letter indicates the direction of propagation and the second one the direction of polarization. An orthorhombic medium can be represented by a system of fractures disposed perpendicular to the isotropic planes of a VTI background medium, as displayed in Fig. 1.

To simplify the characterization of a VTI medium, Thomsen [36] introduced three parameters, which are a combination of the components of the medium's stiffness tensor. They are called anisotropy or Thomsen parameters and are given by the following expressions:

$$\epsilon = \frac{C_{11} - C_{33}}{2C_{33}}, \quad (2)$$

$$\gamma = \frac{C_{66} - C_{44}}{2C_{44}}, \quad (3)$$

and

$$\delta = \frac{(C_{13} + C_{44})^2 - (C_{33} - C_{44})^2}{2C_{33}(C_{33} - C_{44})}, \quad (4)$$

where ϵ and γ are related to the P- and S-waves respectively, while δ is related to both P- and S-waves.

All these parameters can be rewritten in terms of P- and S-wave velocities. Considering an orthorhombic medium and following the same idea of Thomsen's work for VTI media, Tsvankin [39] settled three parameters for each symmetry plane of an orthorhombic medium using the similarities between the TI media and the symmetry planes of the orthorhombic media. Hence, [39] chose the Z-axis as the reference axis for both [X,Z] and [Y,Z] planes and the X-axis for the [X,Y] plane, so he could determine the normal P- and S-wave velocities of reference. Using Christoffel equation,

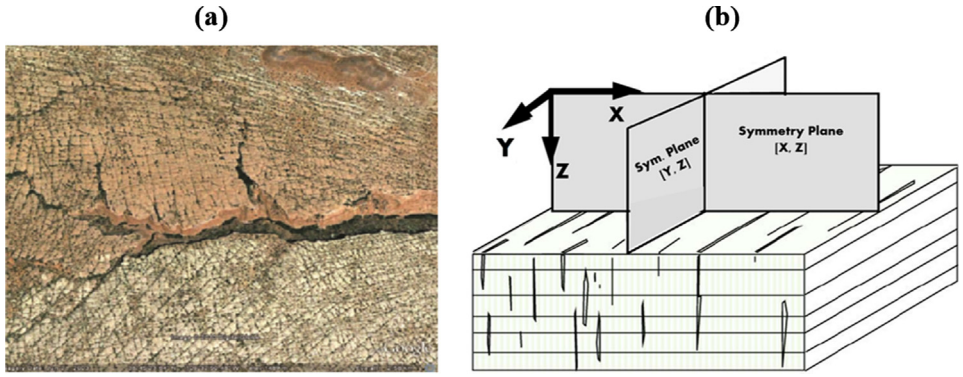

Fig. 1. (a) Example of a real orthorhombic (top) and monoclinic (bottom) sandstone fractured, Arches National Monument. This picture is from Far et al. [16]. (b) Illustration of an orthorhombic medium composed by a vertical fracture swarm in a VTI background. This figure was modified from Tsvankin [39].

$$[G_{ik} - \rho V^2 \delta_{ik}] U_k = 0, \tag{5}$$

which relates the stiffness tensor components of the medium to the phase velocities and the wave propagation directions, he introduced three parameters for each symmetry plane of an orthorhombic medium. The parameters related to the [X,Z] plane are

$$\epsilon_2 = \frac{C_{11} - C_{33}}{2C_{33}}, \tag{6}$$

$$\gamma_2 = \frac{C_{66} - C_{44}}{2C_{44}}, \tag{7}$$

and

$$\delta_2 = \frac{(C_{13} + C_{55})^2 - (C_{33} - C_{55})^2}{2C_{33}(C_{33} - C_{55})}. \tag{8}$$

The ones related to the [Y,Z] plane are

$$\epsilon_1 = \frac{C_{22} - C_{33}}{2C_{33}}, \tag{9}$$

$$\gamma_1 = \frac{C_{66} - C_{55}}{2C_{55}}, \tag{10}$$

and

$$\delta_1 = \frac{(C_{23} + C_{44})^2 - (C_{33} - C_{44})^2}{2C_{33}(C_{33} - C_{44})}. \tag{11}$$

Finally, the ones related to the [X,Y] plane:

$$\epsilon_3 = \frac{C_{22} - C_{11}}{2C_{11}}, \tag{12}$$

$$\gamma_3 = \frac{C_{44} - C_{55}}{2C_{55}}, \tag{13}$$

and

$$\delta_3 = \frac{(C_{12} + C_{66})^2 - (C_{11} - C_{66})^2}{2C_{11}(C_{11} - C_{66})}. \tag{14}$$

Note that the parameters are numbered according to the direction perpendicular to the plane of symmetry analyzed. Using this recipe, the characterization of this kind of medium is simplified being necessary only the measurement of the reference velocities and the calculation of the first 6 parameters [39].

3. Methodology

3.1. Physical models construction

We constructed a total of six models, being one unfractured with VTI symmetry and five fractured orthorhombic models. The orthorhombic symmetry was reached by creating a set of vertical square-shaped fractures on a VTI background. This background in all the models has a total of twelve layers, with the top and bottom layers having a fixed thickness of 1 cm and the ten layers betweem them having 0.4 cm each. The orthorhombic models differ from each other by the number of fractures in their composition, ranging from three (Ortho-1) to seven fractures (Ortho-5). The overall characteristics of the fractures and the VTI background are depicted in Table 1.

For a heterogeneous medium to be considered effectively homogeneous anisotropic, the wavelength of a wave propagating through it needs to be bigger than the inhomogeneities of this medium, some values of the minimum ratio between wavelength and inhomogeneity dimension to consider the medium as effectively anisotropic are defined in various works, as Marion et al. [25] which argues this ratio must be ten, Liner and Fei [23] which states the value must be five and Helbig [19] which argues the ratio must be three. At the present work, our wavelength-to-inhomogeneity ratio for vertical heterogeneities (cracks) is well inside this limits, even for the smallest wavelengths, but for horizontal heterogeneities (layers) – for the smallest wavelengths – we're a bit off the limits, but even so we expect an approximately effectively anisotropic behavior for waves propagating in the Z-direction of the samples, and expect very surely that the vertical inhomogeneities do produce an effectively anisotropic behavior for waves propagating in the X- and Y-directions. In this work, the smallest P-wave wavelength-to-inhomogeneity (layer width) ratio for the Z-direction is 1.95 and the smallest P-wave wavelength-to-inhomogeneity (fracture width) ratio for the X-direction is 8.25. Backus [5] stated that a set of very thin horizontal layers behave as an effective medium of VTI anisotropy, hence, following the same idea, thin vertical layers behave as a HTI medium. Therefore, by generating horizontal layers of thickness equal to 0.4 cm and vertical fractures of width equal to 0.08 cm, we are assuming that the samples generated have orthorhombic anisotropy.

We constructed the physical models based on the methodology proposed by Santos et al. [31], which uses a mixture of fine sand, cement and a small amount of water to manufacture the background of the models and the dissolution of thin slices of styrofoam to produce the fracture system. The proportion of solid material used in all the models

Table 1
Fracture physical parameters of the models.

Model/Property	REF	Ortho-1	Ortho-2	Ortho-3	Ortho-4	Ortho-5
Fracture width (cm)	0	0.08	0.08	0.08	0.08	0.08
Fracture Area (cm^2)	0	4	4	4	4	4
Number of fractures (cm)	0	3	4	5	6	7
Distance between fractures (cm)	–	0.5	0.5	0.4	0.2	0.2
Layer spacing (cm)	0.4	0.4	0.4	0.4	0.4	0.4
Fracture Density (%)	–	2.780	3.540	4.393	5.74	5.792

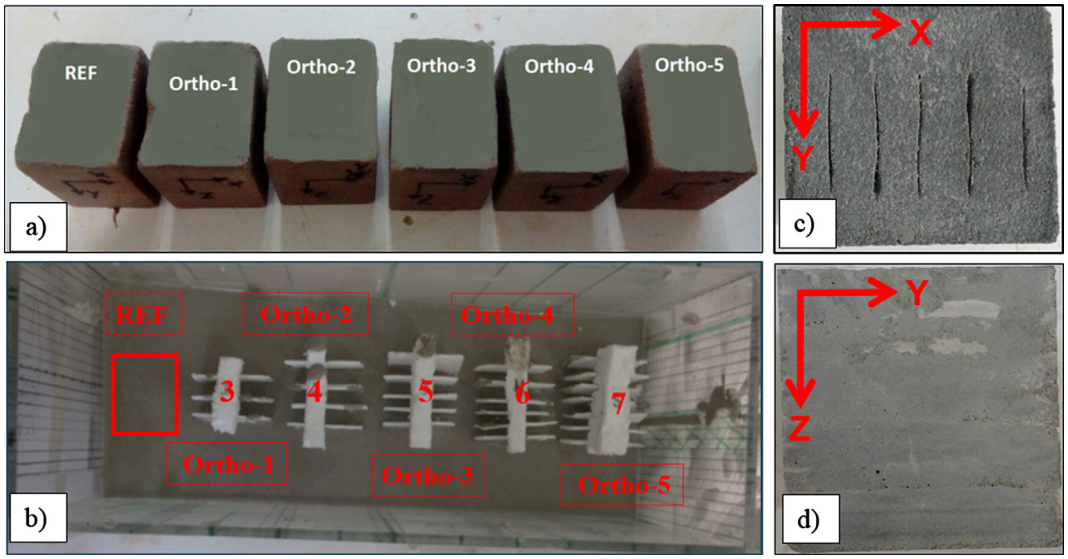

Fig. 2. Representation of the samples construction process: (a) VTI and orthorhombic models; (b) the acrylic mold containing styrofoam cuts included in the first layer deposited; (c) a photo of fracture swarm and (d) an image of the background layering.

was 70% of sand and 30% of cement. The first step was to create the VTI background (Fig. 2d). This is done by inserting the mixture of sand, cement and water in an acrylic mold until the formation of a layer with the predefined thickness is complete. This procedure is repeated, from half an hour to half an hour, until the desired number of layers is produced. To produce the fracture system of the orthorhombic models, we placed squared styrofoam cuts perpendicular to the first layer of deposition, as can be seen in Fig. 2b)]. As said before, the number of cuts varies from model to model ranging from 3 to 7. The pieces of styrofoam are square-shaped with side dimension of 4 cm and width of 0.08 cm. The spacing between them differs, being 0.2 cm the smallest spacing and 0.5 the largest.

After depositing the layers and placing the styrofoam cuts in all models, they are left to dry for about ten hours. Once they are solid, we sprayed water on them twice a day for eight days in order to achieve the maximum Young Modulus as stated by [18], a step called curing process. After this step, in order to make the models even more rigid, we placed them into an oven for about two hours. The last step is to immerse the models into paint thinner for about five hours in order to achieve the complete styrofoam's cuts dissolution. This procedure provides the generation of empty spaces of the same shape of the cuts, thus, the creation of the physical models' fracture system (see Fig. 2c). The resulting samples are displayed in Fig. 2a. The physical and petrophysical properties of the physical models are depicted in Table 2.

3.2. Ultrasonic measurements

We performed ultrasonic measurements on each model through a pulse transmission technique using the Ultrasonic Research System at LPRF. The system consists of: a pulse-receiver 5072PR and pre-amplifier 5660B from Olympus, a pair of ultrasonic transducers, one acting as a source, with a peak frequency of 500 kHz, and the other as the receiver, and an USB oscilloscope of 50 MHz from Handscope. The transmission technique consists in the generation of an ultrasonic pulse by the source. This pulse travels through the model in the desired direction of measurement and is detected by the receiver. The output of each transmission is a waveform representing the arrivals of each wave traveling within the model. From the waveforms we were able to estimate the first arrivals of both P- and S-waves. The Ultrasonic Measurement System used to acquire the waveforms of Fig. 4 is displayed in Fig. 3. Using the first arrivals and the knowledge about the dimensions of each model we were able to obtain P- and S-wave velocities by the following relation:

$$V_{P,S} = \frac{L}{t_{P,S} - t_{delay}}, \tag{15}$$

where L is the sample dimension in the measurement direction, $t_{P,S}$ is the first arrival of the P- or S-wave modes and t_{delay} is the intrinsic delay time of the transducers, in this case, 0.14 μs. This intrinsic delay is due to the coating at the face of the transducer crystal. The sampling rate per channel for all measurements of P and S-wave records was 0.05 μs.

The first step of the measurement procedure was to define the directions on which the waveform acquisition would be realized on each model. We labeled the direction perpendicular to the fractures as the X-direction, parallel to the fractures as the Y-direction and perpendicular to the bedding planes as the Z-direction. They can be more easily visualized in Fig. 2. The transmission procedure was performed in each of these directions. The traveltime pickings were made manually and based on the waveforms only. In the case of fractured media, due to the presence of coda waves, the waveform recordings are in fact very complicated [17]. This problem becomes worse, because as the size of the samples get bigger, there is more scattering inside them. So, as the method applied for picking the wave arrivals is completely visual and manual, the waveform recording of the REF sample (in which the P- and S-wave arrivals are clearer) was used to help distinguishing the S-wave from the P-wave in the other recordings. So, in each recording, it was tried to identify the P-wavepackts, their ends, and then another wavepacket emerging with a different pattern. We consider that the error in the process of manual picking is 0.02 μs.

P-wave velocities were calculated for all transmission directions and defined as Vp_x, Vp_y and Vp_z. Besides, in each direction of propagation we

Table 2
Physical and petrophysical properties of the models.

Model/Property	REF	Ortho-1	Ortho-2	Ortho-3	Ortho-4	Ortho-5
X (cm)	4.286	5.670	5.700	5.920	5.850	5.982
Y (cm)	5.528	4.482	4.673	4.515	4.415	4.870
Z (cm)	5.436	5.436	5.430	5.451	5.180	5.310
Volume (cm^3)	128.795	138.145	144.634	145.699	133.788	154.693
$Mass_{dry}$ (g)	246.080	251.600	252.970	250.580	223.450	258.790
ρ (g/cm^3)	1.911	1.821	1.749	1.720	1.670	1.673
$Mass_{sat}$ (g)	265.75	274.31	278.56	280.99	253.08	295.3
ϕ (%)	15.27	16.44	17.69	20.87	22.15	23.60

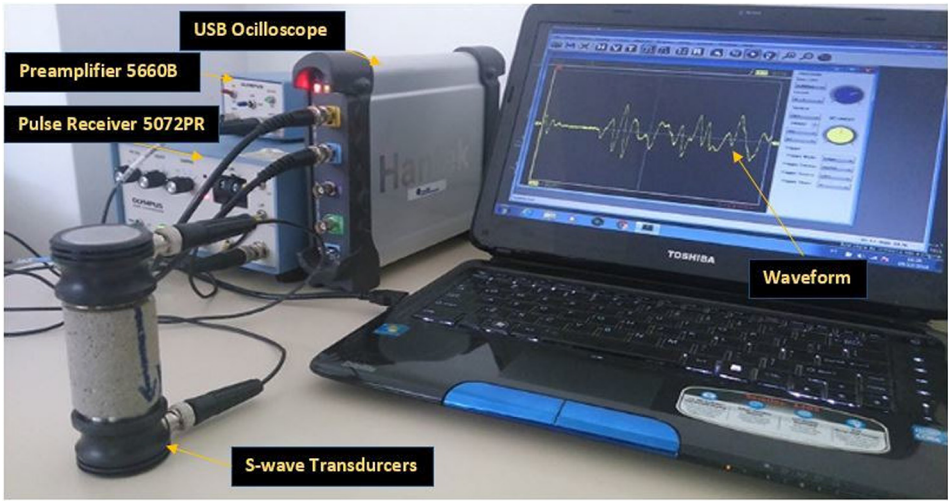

Fig. 3. Ultrasonic measurement system composed by a pulse receptor – model 5072PR and a preamplifier model 5660B- both of Olympus, a 50 Hz USB oscilloscope of Handscope and S-wave transducers of 500 kHz which provide P- and S-waves waveforms.

estimated the velocities of two modes (different polarizations) of S-wave vibration. In the X-direction we calculated the S-wave velocities for waves polarized in the directions Y (Vs_{xy}) and Z (Vs_{xz}). We performed the same procedure for the Y-direction by calculating S-wave velocities for waves polarized in the directions X (Vs_{yx}) and Z (Vs_{yz}). The same was performed for the Z-direction in which we estimated Vs_{zx} and Vs_{zy}.

The velocities, in turn, where used to calculate Tsvankin parameters. In order to write Tsvankin parameters as function of the velocities we specialized Eq. 5 for different phase angles θ, which gives us velocities as function of stiffness coefficients, these relations can be inverted and substituted in Eqs. (6)–(14). For the [X,Z] and [Y,Z] planes, Z-direction was taken as reference, which means $\theta = 0^{\circ}$ when the wave is propagating in the Z-direction and $\theta = 90^{\circ}$ when propagating either in the X- or Y-directions. For the [X,Y] plane, X-direction was chosen to be the reference axis. With the resulting relations, we replaced the stiffness coefficients by the respective velocities found for each of them. The final equations for the ϵ and γ parameters are placed below:

$$\epsilon_1 = \frac{(Vp_y^2 - Vp_z^2)}{2Vp_z^2}, \tag{16}$$

$$\epsilon_2 = \frac{(Vp_x^2 - Vp_z^2)}{2Vp_z^2}, \tag{17}$$

and

$$\epsilon_3 = \frac{(Vp_y^2 - Vp_x^2)}{2Vp_x^2}. \tag{18}$$

$$\gamma_1 = \frac{(Vs_{xy}^2 - Vs_{xz}^2)}{2Vs_{xz}^2}, \tag{19}$$

$$\gamma_2 = \frac{(Vs_{yz}^2 - Vs_{yz}^2)}{2Vs_{yz}^2}, \tag{20}$$

and

$$\gamma_3 = \frac{(Vs_{zx}^2 - Vs_{zy}^2)}{2Vs_{zy}^2}. \tag{21}$$

In this work, we limited ourselves to calculate ϵ and γ parameters, since we were not able to acquire data for waves propagating diagonally in the models (45°).

4. Results

As mentioned before, we estimated the P- and S-wave velocities from the dimensions of the samples and the first arrivals of the waves. These first arrivals were picked from the waveforms generated by the wave transmission process performed in each samples. Fig. 4 shows the waveforms acquired in all directions of the reference and Ortho-1 samples and the first arrival picking of all the waveforms recorded on them.

Table 3 shows all the calculated velocities of both P- and S-waves. Analyzing the P-wave velocity values we can see that Vp_x and Vp_y are different for all the orthorhombic models. It also can be noticed that the P-wave velocity is highly affected by the presence of fractures, since there is a decrease in its values as the number of fractures increases. As expected, this effect is more noticeable in the direction perpendicular to the fractures, the X-direction. In this direction the difference between P-wave velocity for the reference model and model Ortho-5 is approximately 995.8 m/s, representing a decrease of 27.5% of the average value.

By observing the S-wave velocity values we can notice the velocity differences between the S-wave polarized in the X-direction and the one polarized in the Y-direction for all the orthorhombic models, while for the reference model they are equal. Additionally, Vs_{xy} values are similar to Vs_{yx} just like Vs_{zy} is similar to Vs_{yz} and Vs_{zx} is similar to Vs_{xz} for all orthorhombic models. The biggest difference between Vs_{xy} and Vs_{yx}, Vs_{zy} and Vs_{yz}, and Vs_{zx} and Vs_{zx} are 64.5 m/s, 69.1 m/s and 102.4 m/s, which represents errors of 3.2%, 3.5% and 7.05% of the average values, respectively. Another aspect of the data that follows the theory for an S-wave propagating in an orthorhombic medium is the relation between the S-wave velocity values in different directions of polarization: the velocities of the S-wave polarized in the Y-direction are greater than the ones for the S-waves polarized in the X- or Z-direction.

The ϵ and γ parameters obtained for each symmetry plane are shown in Table 4. The values of both parameters certify the statements made in the last paragraph. As expected, the smallest value of ϵ_3 is the one of the reference model and, relative to ϵ_1 and ϵ_2, ϵ_3 presents the biggest values for all the models. Following the same trend as the ϵ parameters, the smallest value of γ_3 is for the reference model. In addition to that, in general, ϵ_2 and γ_2 are intermediate values. It is important to emphasize that for the orthorhombic samples ϵ_2 and γ_2 values are negative.

Fig. 5 shows a representation of the model indicating the directions of measurement along with the results obtained for the P-wave velocities and the absolute values of the ϵ parameters. Observe that the

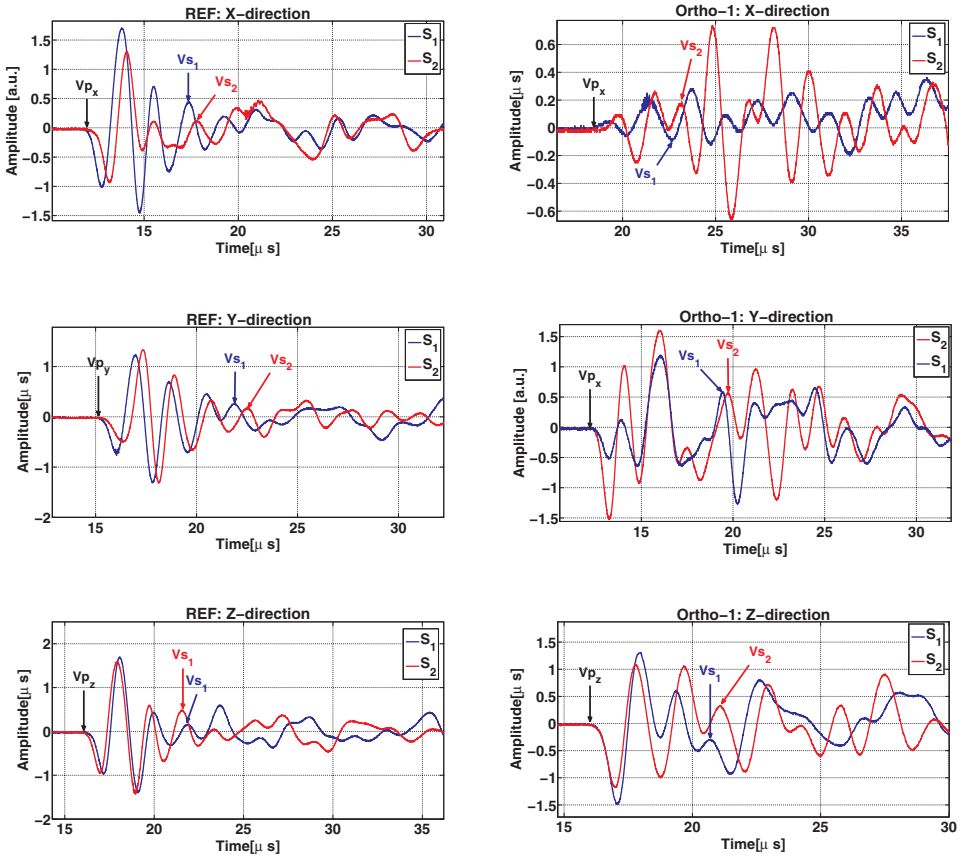

Fig. 4. Examples of manual travel time picking of both P- and S-waves. The left column shows the waveforms related to the reference samples, whereas the right column shows waveforms related to sample Ortho-1. Notice the increase in travel time difference in the Z-direction from one model to the other showing the increase of the S-wave birefringence due to the presence of the fractures.

linear trend and the fitting equations of the velocities and ϵ values are also displayed in the plots. Also, it can be noticed that, unlike the other ϵ values, ϵ_1 slightly decreases as the number of fracture increases. Notice that for a low number of fractures ϵ_2 also decreases.

Fig. 6 shows a representation of the models indicating the direction of measurement together with the S-wave velocity and γ plots. The results show that the S-wave velocity, γ_1 and γ_3 values follow a quadratic trend, while γ_2 values follow a linear trend. The fitting equation of the velocities and γ values is exhibited in each plot. Notice that the rate of increase of γ_1 parameter is smaller than the rate of the other γ values and that its values start to decrease for the highest number of fractures.

5. Discussions

The acquired waveforms, velocities and parameters certify the benefits of the presented construction methodology. All velocity trends are consistent with the theory behind wave propagation in orthorhombic medium with the crack system placed in the [Y,Z] plane. As can be noticed in the results, Vp_y is greater than Vp_z and Vp_z is greater than Vp_x for all the physical models, suggesting that the fracture contribution for anisotropy is greater than the contribution of the layered background. Also, the decrease on the P-wave velocity values of the Y- and Z-directions – with the increase of the number of fractures – agree with the theory of elastic waves propagating along a displacement discontinuity or a compliant surface studied by Pyrak-Nolte et al. [28]. Besides, the fracture surfaces are not smooth which causes a decrease on the stiffness of the fractures and that, in turn, generates a delay on

Table 4
Tsvankin parameters as a function of the number of fractures.

Tsvankin Parameter (%)	REF	Ortho-1	Ortho-2	Ortho-3	Ortho-4	Ortho-5
ϵ_1	6.87	7.12	6.49	6.77	5.84	5.35
ϵ_2	6.87	−4.35	−4.81	−7.84	−11.22	−13.03
ϵ_3	0.0	12.57	12.50	17.34	22.01	24.86
γ_1	8.2	9.34	10.57	11.00	10.17	9.04
γ_2	8.2	−2.55	−9.24	−11.08	−16.42	−17.94
γ_3	0.0	16.32	19.00	22.61	32.59	38.87

Table 3
P-wave and S-wave velocity results from manual picking.

Elastic velocity (m/s)	REF	Ortho-1	Ortho-2	Ortho-3	Ortho-4	Ortho-5
Vp_x	3626.7	3091.603	3004.744	2850.265	2707.080	2627.141
Vp_y	3626.7	3458.333	3359.454	3307.692	3248.712	3214.521
Vp_z	3402	3235.714	3160.651	3104.214	3074.183	3055.235
Vs_{xy}	2227.3	2045.6	1900.4	1822.8	1667.9	1522.8
Vs_{xz}	2065.4	1877.7	1726.6	1650.3	1520.4	1401.4
Vs_{yx}	2227.3	1981.1	1851.3	1772.5	1615.1	1550.1
Vs_{yz}	2065.4	2033.7	2050.6	2009.2	1971.1	1935.8
Vs_{zx}	2065.4	1792.6	1768.0	1695.3	1579.4	1503.8
Vs_{zy}	2065.4	2064.5	2076.9	2043.0	2029.9	2004.9

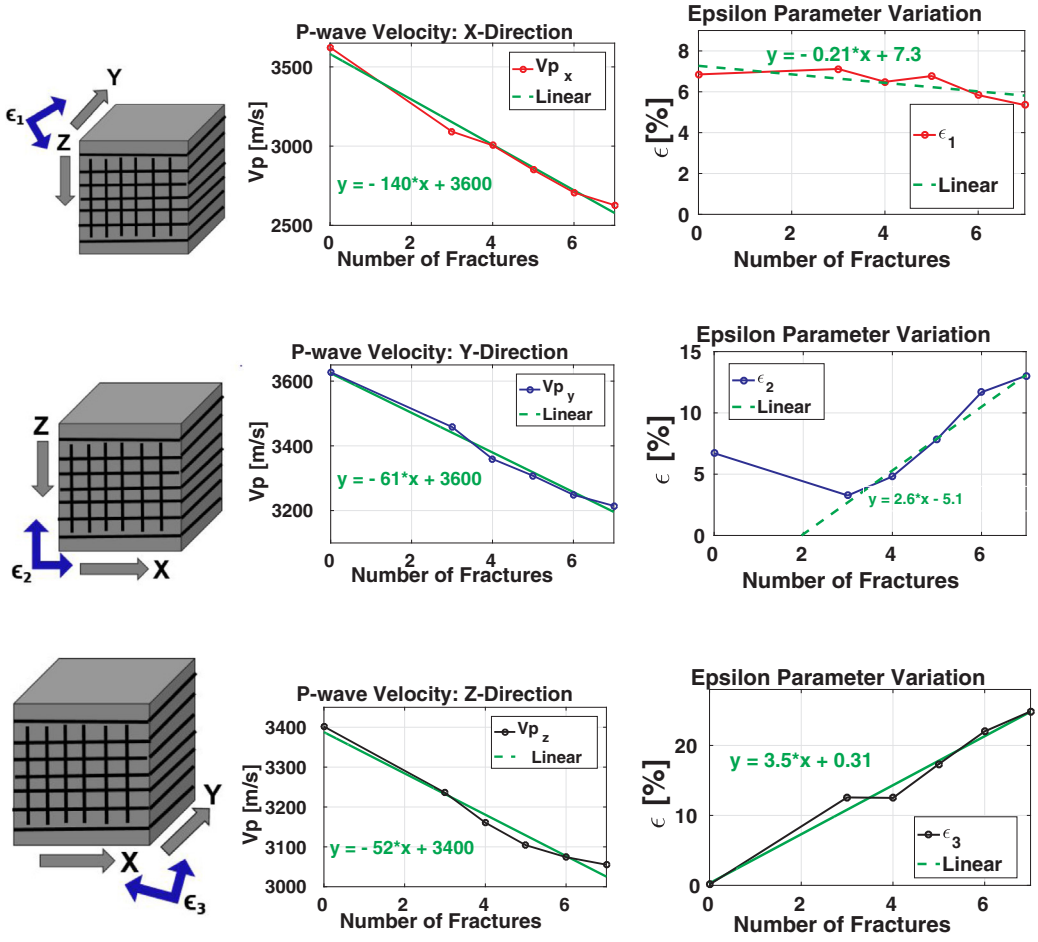

Fig. 5. P-wave velocity and ϵ parameter variation as function of number of cracks: the figures in the column to the left illustrate samples highlighting the directions of measurement related to the velocities used to calculate the Epsilon parameters, the plots in the middle column display the P-wave velocities in the X-, Y- and Z-direction, respectively, and the ones in the column to the right present ϵ_1, ϵ_2 and ϵ_3 variation.

the arrival time of the wave propagating along the fracture (the [Y,Z] plane, in our case). This anisotropic phenomenon is explained by Pyrak-Nolte and Cook [27] for Rayleigh waves, but from the results presented here this phenomenon is also applicable for P-waves.

The parameters ϵ_2 and ϵ_3 increased as function of the number of fractures. We observed a decrease in ϵ_2 values for a low number of fractures and that can be explained by analyzing the anysotropic effects responsible for the delay time of the P-wave velocities for X- and Z-directions. Its noticeable that the rate of decrease of the *Vp* values for the X-direction is greater than the rate of decrease for the Z-direction. These decrease for the P-wave velocity values in the Z-direction causes a decrease in the squared-velocity difference used to calculate the ϵ_2 values, which can be seen for the first two orthorhombic samples, Ortho-1 and Ortho-2, whose ϵ_2 values are smaller than the value for the VTI sample. For the samples with higher number of fractures, this squared-velocity difference is bigger due to the greater decrease rate of the P-wave velocity values in the X-direction. Then, analyzing the samples degree of anisotropy by only considering the ϵ_2 values can be misleading because it indicates that the samples Ortho-1 and Ortho-2 are less anisotropic than the *REF* sample, which is a false statement. We hipotesize that for a low number of fractures the effect of the wave propagating along a fracture and the effect of the wave propagating perpendicular to the fractures camouflage each other, and that for a high number of fractures the effect of the wave propagating perpendicular to the fracture stands out.

For the X-direction, Vs_1 – S-wave polarized longitudinally to the layers – and Vs_2 – S-wave polarized transversely to the layers – decrease with the same rate due to the effect of the cracks in the direction of propagation. Notice that the Vs_2 values are, in general, smaller than the Vs_1 values, which indicates that not only the wave-travelling-along-a-fracture effect is accounting to the arrival time delay but also the layered background. For the Y-direction, both Vs_1 – S-wave polarized transversely to the layers – and Vs_2 – S-wave polarized transversely to the fracture system – also decrease as function of the number of fractures due to the effect of a wave propagating along a fracture in the direction of propagation, however they decrease with different rates: Vs_2 decreases more quickly than Vs_1 due to the fractures effect. For the Z-direction, the S-wave velocity values have the same behavior observed for the Y-direction, but the outstanding rate of Vs_2 means that the wave polarized across the fractures is more affected by the anisotropy caused by the fractures. As consequence of the S-wave velocities behavior, γ_1 values are the smallest and γ_3 values are the greatest, and both increase as a function of the number of fractures. In addition, γ_1 presents a small rate of variation in comparison to the other γ's. The γ_1 values being positive implies that although the anisotropy effect on Vs_1 is noticeable, this effect on Vs_2 is greater and that is also a likely result.

Based on both P- and S-wave velocities behavior described in the last paragraphs, it is reasonable to state that the effect of a wave propagating along a fracture is the one that causes the smallest time delay on the wave arrival time, followed by the effect of the layered background and the effect of a wave travelling across the fractures, respectively. This is ensured by γ_3 and ϵ_3, the parameters relative to the difference between the effect of a wave travelling across the fractures (the greatest effect) and the effect of a wave propagating along a

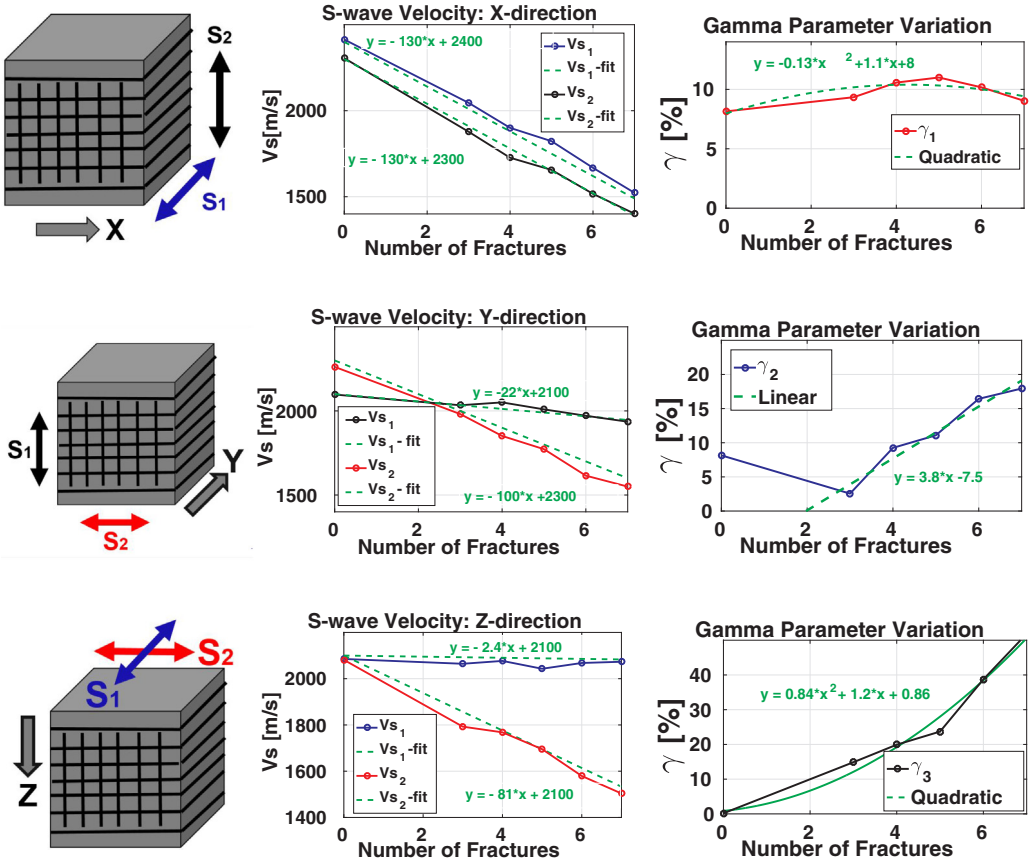

Fig. 6. S-wave velocity and γ parameter variation as function of number of fractures: the figures in the column to the left illustrates a sample highlighting the directions of propagation and polarization related to the velocities used to calculate the Gamma parameters, the plots in the middle column displays the S-wave velocities in the X-, Y- and Z-direction, respectively, and the ones in the column to the right present γ_1, γ_2 and γ_3 variation.

fracture (the smallest effect), presenting the biggest values.

Even though it is not the goal of this work to find a relationship between Tsvankin's parameters, we performed a correlation between them in order to identify (if it does exist) a number of fracture window in which we can estimate one parameter by knowing the value of one of the others. Fig. 7 is showing the correlation plots between the parameters γ and ϵ estimated from the ultrasonic measurements. First of all, the γ values in all directions plotted against ϵ_1 show a opposite behavior in comparison with the plots against ϵ_2 and ϵ_3. For all the values of γ we see that the curves have a linear behavior, i.e. γ and ϵ have a high correlation, for small number of fractures (lower than 5). For higher number of fractures, the relationships depicted in the figures become nonlinear.

6. Conclusions

From the construction of porous orthorhombic physical models and their characterization from ultrasonic measurements, we estimated the elastic velocities, calculated the anisotropy parameters, and presented correlations between Tsvankin parameters (ϵ and γ) for all orthogonal directions of measurement. Based on our results, we can state the following conclusions:

- The methodology presented here is practical, inexpensive and successful on making orthorhombic models with a VTI background and a fracture system. Additionally, using this methodology the fracture system can be placed in any direction and also it can be constituted by any number of fractures of the researcher's choice. In conjunction to that, all the models are porous and that creates the possibility of evaluating the P- and S-wave velocities behavior in a saturated medium kinematically more similar to Earth's sedimentary rocks;
- Both P- and S-wave velocities are directly affected by the increase of empty spaces generated by the styrofoam dissolution. These velocity values present a inversely proportional behavior in relation to the number of fractures;
- The fractures generated by this methodology cause time delays in both the in-plane and out-of-plane directions to the fracture orientation, however this time delay is more apparent in the wave perpendicularly propagating to the fracture plane. This means even though the fracture surface is not smooth, the rugosity effect is smaller than the effect caused by a wave traveling through a displacement discontinuity, e.g. a fracture;
- The anisotropic effect of the VTI background and the effect caused by the presence of the fractures cancel out for small number of fractures and this phenomena is noticeable in the ϵ_2 parameter. The elastic velocity, the ϵ's and the γ_Y presented a linear relationship with the number of fractures while γ_X and γ_Z presented a quadratic relationship with it. Each ϵ parameter is highly correlated with each γ parameter for a number of fractures lower than 5. After that point, the correlations curves are nonlinear.

For further works, it following the same procedures presented in this article, we can perform other experiments with the orthorhombic media or more complex media, such as media with monoclinic or triclinic symmetry. Also, we can saturate the physical models with different fluids and analyze the behavior of the elastic properties, e.g. elastic velocities and compliance.

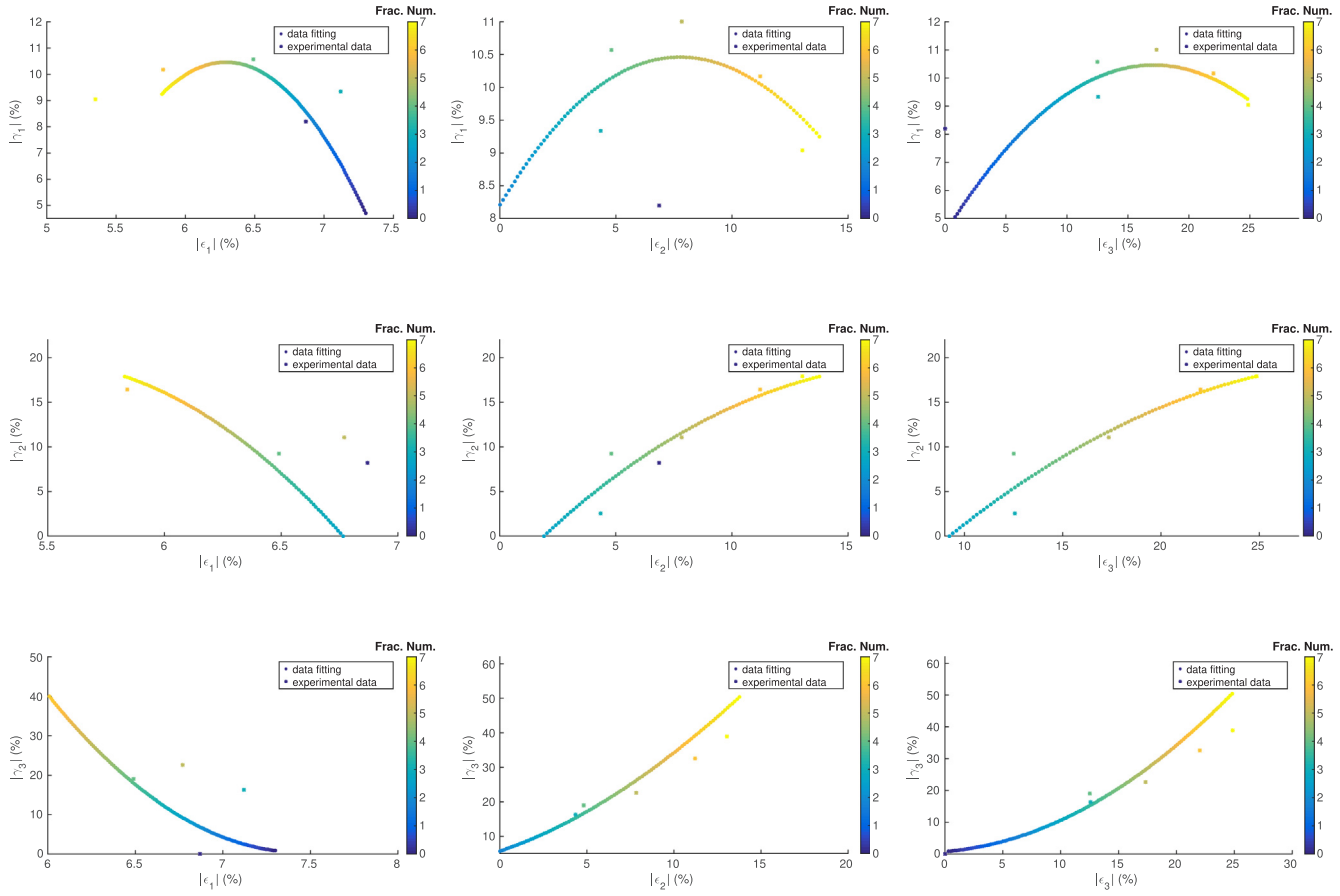

Fig. 7. In the top: correlation between the γ_1 parameter and ϵ's (ϵ_1, ϵ_2, ϵ_3) parameters. In the medium: correlation between the γ_2 parameter and ϵ's parameters. In the bottom: correlation between the γ_3 parameter and ϵ's parameters. As can be observed, all epsilons are correlated to all gammas for a number of fractures lower than 5.

Acknowledgments

The construction of the synthetic physical models as well as the ultrasonic measurements were carried out at the Laboratory of Petrophysics and Rock Physics – Dr. Om Prakash Verma (LPRP) at the Federal University of Para, Brazil. The authors would like to thank PET/GEOFÍSICA-UFPA-Ministério da Educação, INCT-GP and CNPq (Grant No.: 459063/2014-6 and Grant No.: CNPQ 140174/2016-8) from Brazil and the Geophysics Graduate Program at Federal University of Pará for the financial support in this research. The authors also would like to thanks the reviewer and editor by the essential comments on the revision.

Appendix A. Supplementary material

Supplementary data associated with this article can be found, in the online version, at https://doi.org/10.1016/j.ultras.2018.11.015.

References

[1] K. Amalokwu, A.I. Best, J. Sothcott, M. Chapman, T. Minshull, X.-Y. Li, Water saturation effects on elastic wave attenuation in porous rocks with aligned fractures, Geophys. J. Int. 197 (2) (2014) 943–947.
[2] J. Assad, R. Tatham, J. McDonald, A physical model study of microcrack-induced anisotropy, Geophysics 57 (12) (1992) 1562–1570.
[3] J.M. Assad, The effect of orthorhombic anisotropy and its implication for oil recovery and reservoir exploitation, Geophys. Prospect. 53 (1) (2005) 121–129.
[4] J.M. Assad, J.A. Mcdonald, R.H. Tatham, T.M. Kusky, Elastic wave propagation in a medium containing oriented inclusions with a changing aspect ratio: a physical model study, Geophys. J. Int. 125 (1) (1996) 163–172.
[5] G.E. Backus, Longwave elastic anisotropy produced by horizontal layering, J. Geophys. Res.: Solid Earth 67 (1962) 4427–4440.
[6] R.J. Brown, D.C. Lawton, S.P. Cheadle, Scaled physical modelling of anisotropic wave propagation: multioffset profiles over an orthorhombic medium, Geophys. J. Int. 107 (3) (1991) 693–702.
[7] C. Chang, G.H.F. Gardner, Effects of vertically aligned subsurface fractures on seismic reflections: a physical model study, Geophysics 62 (1) (1997) 245–252.
[8] S. Cheadle, R. Brown, D. Lawton, Orthorhombic anisotropy: A physical seismic modeling study, Geophys. Res. Lett. 56 (10) (1991) 1603–1613.
[9] S. Crampin, A review of wave motion in anisotropic and cracked elastic-media, Wave Motion 3 (4) (1981) 343–391.
[10] S. Crampin, R. Evans, B. Üçer, M. Doyle, J.P. Davis, G.V. Yegorkina, A. Miller, Observations of dilatancy-induced polarization anomalies and earthquake prediction, Nature 286 (5776) (1980) 874.
[11] J.J.S. de Figueiredo, J. Schleicher, R.R. Stewart, N. Dyaur, Estimating fracture orientation from elastic-wave propagation: an ultrasonic experimental approach, J. Geophys. Res.: Solid Earth 117 (B8) (2012) B08304.
[12] P. Ding, B. Di, D. Wang, J. Wei, X. Li, P and S wave anisotropy in fractured media: experimental research using synthetic samples, J. Appl. Geophys. 109 (Supplement C) (2014) 1–6.
[13] P. Ding, B. Di, J. Wei, X. Li, Y. Deng, Fluid-dependent anisotropy and experimental measurements in synthetic porous rocks with controlled fracture parameters, J. Geophys. Eng. 11 (1) (2014) 015002.
[14] A. Ekanem, J. Wei, X.-Y. Li, M. Chapman, I. Main, P-wave attenuation anisotropy in fractured media: a seismic physical modelling study, Geophys. Prospect. 61 (2013) 420–433.
[15] A.M. Ekanem, X.Y. Li, M. Chapman, M. Ian, J. Wei, Effect of fracture aperture on P-wave attenuation: a seismic physical modelling study, Int. Sch. Res. Notices (ISRN) Geophys. (2014) Article ID 241279, http://dx.doi.org/10.1155/2014/241279.
[16] M.E. Far, C.M. Sayers, L. Thomsen, D. Han, J.P. Castagna, Seismic characterization of naturally fractured reservoirs using amplitude versus offset and azimuth analysis, Geophys. Prospect. 61 (2) (2013) 427–447.
[17] J. Figueiredo, J. Schleicher, R. Stewart, N. Dyaur, Estimating fracture orientation from elastic-wave propagation: an ultrasonic experimental approach, J. Geophys. Res.: Solid Earth (2012) 117 B8.
[18] Garcia, G.C.R., B., S.E.M., S., R., 03 2011. Efeito do tempo de cura na rigidez de argamassas produzidas com cimento Portland. Cerâmica 57, 94–99.
[19] K. Helbig, Anisotropy and dispersion in periodically layered media, Geophysics 49 (4) (1984) 364–373.
[20] J.P. Henriques, J.J.S. de Figueiredo, L.K. Santos, D.L. Macedo, I. Coutinho, C.B. da Silva, A.L. Melo, M. Sousa, F.L. Azevedo, Experimental verification of effective anisotropic crack theories in variable crack aspect ratio medium, Geophys.

Prospect. 66 (2018) 141–156.
[21] J.A. Hudson, Overall properties of a cracked solid, Math. Proc. Cambridge Philos. Soc. 88 (2) (1980) 371–384.
[22] J.A. Hudson, Wave speeds and attenuation of elastic waves in material containing cracks, Geophys. J. Roy. Astron. Soc. 64 (1) (1981) 133–150.
[23] C.L. Liner, T.W. Fei, Layer-induced seismic anisotropy from full-wave sonic logs: theory, application, and validation, Geophysics 71 (6) (2006) D183–D190.
[24] F. Mahmoudian, G. Margrave, P. Daley, J. Wong, D. Henley, Estimation of elastic stiffness coefficients of an orthorhombic physical model using group velocity analysis on transmission data, Geophysics 79 (1) (2013) R27–R39.
[25] D. Marion, T. Mukerji, G. Mavko, Scale effects on velocity dispersion: from ray to effective medium theories in stratified media, Geophysics 59 (10) (1994) 1613–1619.
[26] Nelson, R.A., 1985. Geologic analysis of naturally fractured reservoirs. Gulf Pub. Co. Book Division.
[27] L.J. Pyrak-Nolte, N.G.W. Cook, Elastic interface waves along a fracture, Geophys. Res. Lett. 14 (11) (1987) 1107–1110.
[28] L.J. Pyrak-Nolte, L.R. Myer, N.G.W. Cook, Anisotropy in seismic velocities and amplitudes from multiple parallel fractures, J. Geophys. Res.: Solid Earth 95 (B7) (1990) 11345–11358.
[29] J. Rathore, E. Fjaer, R. Holt, L. Renlie, P-and S-wave anisotropy of a synthetic sandstone with controlled crack geometry, Geophys. Prospect. 43 (6) (1995) 711–728.
[30] L.K. Santos, J.J.S. de Figueiredo, C.B. da Silva, A study of ultrasonic physical modeling of isotropic media based on dynamic similitude, Ultrasonics 70 (2016) 227–237.
[31] L.K. Santos, J.J.S. de Figueiredo, D.L. Macedo, A.L. de Melo, C.B. da Silva, A new way to construct synthetic porous fractured medium, J. Petrol. Sci. Eng. 156 (Supplement C) (2017) 763–768.
[32] L.K. Santos, J.J.S. de Figueiredo, B. Omoboya, J. Schleicher, R.R. Stewart, N. Dyaur, On the source-frequency dependence of fracture-orientation estimates from shear-wave transmission experiments, J. Appl. Geophys. 114 (Supplement C) (2015) 81–100.
[33] Sayers, C., 2007. Seis mic characterization of reservoirs containing multiple fracture sets. In: SEG Technical Program Expanded Abstracts 2007. SEG Technical Program Expanded Abstracts. Society of Exploration Geophysicists, pp. 1456–1460.
[34] D.J. Shuai, B.D. Wei, S. Yaun, J. Xie, S. Yan, Experimental study of fracture size effect on elastic-wave velocity dispersion and anisotropy, Geophysics 83 (2017) C49–C59.
[35] Skjærstein, A., Fjær, E., 2001. Angular dependent attenuation in a sandstone with parallel cracks. In: Advances in Anisotropy: Selected Theory, Modeling, and Case Studies. Society of Exploration Geophysicists, pp. 205–216.
[36] L. Thomsen, Weak elastic anisotropy, Geophysics 51 (10) (1986) 1954–1966.
[37] P. Tillotson, M. Chapman, A.I. Best, J. Sothcott, C. McCann, W. Shangxu, X.-Y. Li, Observations of fluid-dependent shear-wave splitting in synthetic porous rocks with aligned penny-shaped fractures, Geophys. Prospect. 59 (1) (2011) 111–119.
[38] P. Tillotson, J. Sothcott, A.I. Best, M. Chapman, X.-Y. Li, Experimental verification of the fracture density and shear-wave splitting relationship using synthetic silica cemented sandstones with a controlled fracture geometry, Geophys. Prospect. 60 (3) (2012) 516–525.
[39] I. Tsvankin, Anisotropic parameters and P-wave velocity for orthorhombic media, Geophysics 62 (4) (1997) 1292–1309.
[40] Wei, J., Di, B., Li, X., 2007. Effects of fracture scale length and aperture on seismic waves: an experimental study. In: SEG Technical Program Expanded Abstracts 2007. SEG Technical Program Expanded Abstracts. Society of Exploration Geophysicists, pp. 169–173, DOI: 10.1190/1.2792404.